Structural Engineering and Mechanics, *Vol. 70, No. 1 (2019) 43-54*
DOI: https://doi.org/10.12989/sem.2019.70.1.043

Crack analysis of reinforced concrete members with and without crack queuing algorithm

P.L. Ng [*1,2], F.J. Ma[2a] and A.K.H. Kwan[2b]

[1] *Faculty of Civil Engineering, Vilnius Gediminas Technical University, Sauletekio Al. 11, Vilnius LT-10223, Lithuania*
[2] *Department of Civil Engineering, The University of Hong Kong, Pokfulam, Hong Kong, China*

(Received January 17, 2018, Revised November 13, 2018, Accepted February 8, 2019)

Abstract. Due to various numerical problems, crack analysis of reinforced concrete members using the finite element method is confronting with substantial difficulties, rendering the prediction of crack patterns and crack widths a formidable task. The root cause is that the conventional analysis methods are not capable of tracking the crack sequence and accounting for the stress relief and re-distribution during cracking. To address this deficiency, the crack queuing algorithm has been proposed. Basically, at each load increment, iterations are carried out and within each iteration step, only the most critical concrete element is allowed to crack and the stress re-distribution is captured in subsequent iteration by re-formulating the cracked concrete element and re-analysing the whole concrete structure. To demonstrate the effectiveness of the crack queuing algorithm, crack analysis of concrete members tested in the literature is performed with and without the crack queuing algorithm incorporated.

Keywords: concrete cracking; crack queuing algorithm; crack width; finite element analysis

1. Introduction

Due to the challenges posed by crack analysis, the prediction and control of cracks in concrete structures, which could cause serviceability and durability problems, are not easy and are still largely based on empirical rules. Though the finite element method is highly versatile and widely applied in structural design and engineering, crack analysis of concrete structures by the finite element method has been facing enormous difficulties. Among the two crack modelling approaches, namely the smeared crack model and the discrete crack model, each has its own merits but both are seriously hampered by their respective limitations. The smeared crack approach (Rots *et al*. 1985, Ohmenhäuser *et al*. 1998) models cracks by numerically changing the constitutive relation of the cracked concrete such that the axial stiffness perpendicular to the crack and the shear stiffness across the crack are reduced to account for cracking. However, since the strains of the cracked concrete element are dependent on the element size (Bažant and Oh 1983), the element tensile strain could not be directly used to evaluate the crack width. After cracking, some researchers assume that the cracks could rotate (De Borst and Nauta 1985, Willam and Pramono 1987) whereas some other researchers assume that the cracks would not rotate (Rashid 1968, Suidan and Schnobrich 1973, Červenka 1985, Frantzeskakis and Theillout 1989).

The discrete crack approach was proposed by Ngo and Scordelis (1967), who insert crack elements into pre-determined crack locations, and once a crack element satisfies the cracking criterion, the concrete across the crack is sub-divided into separate concrete elements. On the other hand, Nilson (1968) inserts crack elements along the concrete element boundaries. However, these simplifying assumptions may induce large errors if the actual crack paths deviate significantly from the pre-determined crack locations or the concrete element boundries. For better accuracy, adaptive remeshing and insertion of crack elements based on the numerical results are required (Ingraffea and Saouma 1985). However, such adaptive remeshing necessitates renumbering of nodes and elements (Ng *et al*. 2010, Kwan *et al*. 2010), as well as mapping of element stress states from the existing mesh to the new mesh (Bittencourt *et al*. 1996, Yang and Chen 2005). These invoke complicated algorithms in computer programming and demands tremendous computing resources. Therefore, implementation of the discrete crack model with adaptive remeshing has been limited in applications.

When a crack is formed, the stiffness of the cracked concrete would reduce (this is referred to as the tension softening) and the deformation would be concentrated in the cracked concrete (this is referred to as the strain localization). These phenomena would cause stress relief in the uncracked concrete and hence stress re-distribution in the vicinity of the crack. The stress relief and stress re-distribution can be captured in the analysis only if the crack sequence is simulated correctly. This cannot be done by the conventional way of employing either the smeared or discrete crack model in the finite element analysis. The

∗Corresponding author, Ph.D.
E-mail: irdngpl@gmail.com
[a] Ph.D.
E-mail: max.mafj@gmail.com
[b] Professor
E-mail: khkwan@hku.hk

http://www.techno-press.com/journals/sem&subpage=7 ISSN: 1225-4568 (Print), 1598-6217 (Online)

reason is that during the analysis, the external load has to be applied in increments. After a load increment, a number of concrete elements could reach the crack criterion while in reality, the most critical concrete element would crack first and stress re-distribution would immediately occur. If all these elements are allowed to crack simultaneously, the crack sequence and pattern could be far different from the reality. As the crack width is largely dependent on the crack pattern, the crack width prediction by the conventional way of crack analysis is unreliable.

In order to address the above deficiency, the crack queuing algorithm has been proposed (Wang *et al*. 1999, Kwan *et al*. 1999). By virtue of this algorithm, iterations are carried out at each load increment level, and within each iteration step, only one concrete element, which is the most critical element, is allowed to crack, and the stress re-distribution is accounted for by re-formulating the cracked concrete element and re-analysing the whole structure again. After then, the next most critical concrete element is allowed to crack and the iteration is repeated until no more new crack appears. This methodology can allow accurate evaluation of crack patterns, crack spacings and crack widths (Ng *et al*. 2015). In the present research, the crack queuing algorithm is employed in conjunction with the smeared representation of cracks and the non-rotating crack model.

Recently, alternative approaches for crack modelling have been put forward. For example, the extended finite element method (Moës and Belytschko 2002, Bobiński and Tejchman 2012, Roth *et al*. 2013, 2015) enriches the cracked elements by dividing the displacement field of each cracked element into two parts, a continuous part that reflects the deformation of the continuum and a discontinuous part that reflects the deformation across the crack. This allows tracking of crack paths while averting the need of remeshing due to crack propagation. Mesoscopic analysis of concrete by the discrete element method (Schlangen and Van Mier 1992, Schlangen and Garboczi 1997, Chen and Baker 2004, Azevedo *et al*. 2010, Cusatis *et al*. 2010, Eliáš and Stang 2012, Khodaie *et al*. 2016) with the use of a lattice model or a discrete particle model is also viable. At the meso-scale, the paste matrix and aggregate in concrete are modelled separately so that the properties of the aggregate particles and the links connecting the aggregate particles are established according to the properties of the paste matrix and aggregate. During the analysis, the computed crack paths cut through the links to simulate crack initiation and propagation. This method has been widely applied to granular and geo-materials. To account for the interfacial transition zone (ITZ) between paste matrix and aggregate particles in concrete, mesoscopic analysis by the finite element method (Kwan 1999, Chen *et al*. 2013) with employment of interface elements to simulate the ITZ can be performed. It should be noted that mesoscopic analyses based on discrete and finite element methods are computationally very intensive.

The modelling of reinforcing bars has a bearing on the crack analysis because the bond-slip between concrete and reinforcing bars would affect the stress and strain fields near the cracks. In general, the reinforcing bars can be simulated in two ways, namely the smeared bar approach and the discrete bar approach. The former approach superimposes the stiffness of reinforcing bars onto the stiffness of concrete elements (Gupta and Akbar 1984). However, such approach presumes perfect bond and thus the bond-slip could not be allowed for (So *et al*. 2010, Contrafatto *et al*. 2012). The latter approach models the reinforcing bars using discrete bar elements (Jendele and Červenka 2006, Ng *et al*. 2011). This approach offers the possibility of inserting interface elements between the discrete bar elements and the concrete elements to allow for bond-slip. Herein, the discrete bar approach is adopted in conjunction with interface elements for incorporating the bond-slip effects.

However, despite theoretically sound, there has been a lack of research on the effectiveness of the crack queuing algorithm in facilitating crack analysis of reinforced concrete members. This research gap is filled in the present study by conducting crack analysis of concrete members tested in the literature with and without incorporation of the crack queuing algorithm and cross-checking the analytical and experimental results. It will be seen that with the crack queuing algorithm incorporated, the finite element method is now capable of generating a discrete crack pattern with clearly defined crack number, crack spacing and crack width in good agreement with the respective experimental results. Moreover, it is computational much more efficient than the practice of reducing the load increments to avoid formation of closely spaced cracks with unrealistically small crack widths.

2. Finite element procedure

The nonlinear finite element procedure adopted in the present study is the same as that previously developed by the authors (Ma and Kwan 2015, Kwan and Ma 2016), which has been validated by applying to reinforced concrete members subjected to flexure and axial tension and checking against the experimental results. To enable modelling of softening behaviour of materials, the stiffness matrix formulation is based on secant stiffness (Wells and Sluys 2001, Kwan and He 2001). The concrete is modelled by two-dimensional plane stress elements, the reinforcing bars are modelled by one-dimensional bar elements, and the reinforcing bar-concrete bond is modelled by one-dimensional Goodman-type interface elements (Goodman *et al*. 1968) with infinitesimal thickness. The interface element has two pairs of duplicated nodes. Each duplicated nodal pair shares the same coordinates but possesses independent degrees of freedom. The bond slip is calculated from the relative displacements of the nodal pairs along the direction of reinforcing bar. The evaluation of bond slip from the nodal displacements of the interface element had been described in detail previously (Ma and Kwan 2015) and hence is not repeated in this paper.

2.1 Materials modelling

For the concrete, the strength is established from the biaxial strength envelope of Kupfer and Gerstle (1973). To

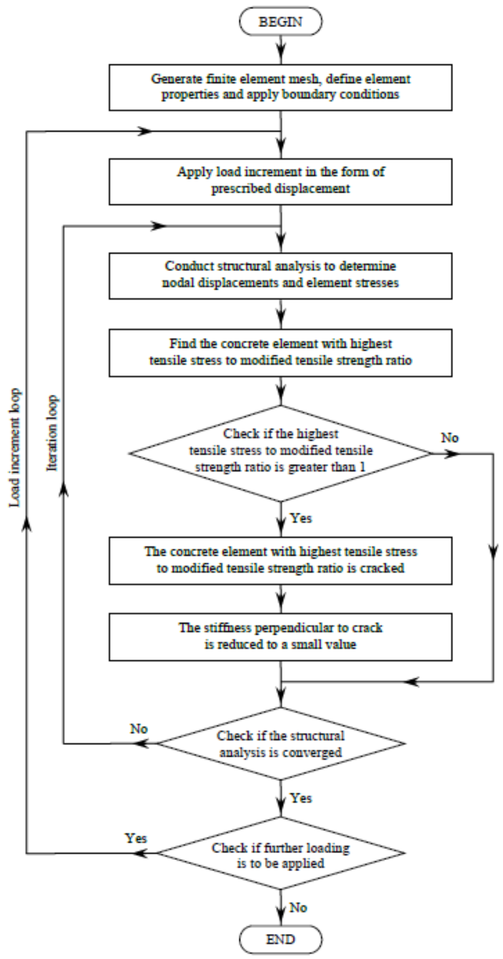

Fig. 1 Flowchart of crack queuing algorithm

transform the biaxial stress-strain relations into uniaxial stress-strain relations in the principal stress-strain directions, the notion of equivalent uniaxial strain (Kwan *et al*. 1999, 2017) is adopted. Under compression, the stress-strain curve by Desayi and Krishnan (1964) is used; whilst under tension, it is assumed that the stress-strain curve is linearly elastic up to cracking and the concrete has no resistance thereafter. Unlike mesoscopic analysis of concrete material comprising of paste matrix and aggregate particles (Wang *et al*. 1999), where very fine finite element mesh in conjunction with nonlinear concrete tensile constitutive model were used, in the present macroscopic analysis which is less inflicted by stress concentration in front of crack tips, a sophisticated tensile constitutive model is not adopted. Nevertheless, as described in detail later, to avoid unstable crack propagation, the fracture toughness of concrete has been incorporated in the tensile constitutive model, though in a simplified way. It should be remarked that there is no conflict between the crack queuing algorithm and the use of any sophisticated concrete tensile constitutive model. If so wished, the crack queuing algorithm can be used in tandem with any concrete tensile constitutive model.

For the reinforcing bars, the stress-strain relation is taken to be elasto-plastic with strain hardening (Mander 1983). For the bond between reinforcing bar and concrete, the bond stress-slip relation is based on that recommended by fib Model Code 2010 (Fédération Internationale du Béton 2013). It should be noted that the initial bond stiffness calculated from the Model Code 2010 formula is infinite large. Herein, the bond stiffness at the initial stage is limited to the secant stiffness at 20% of the peak bond stress (Kwan and Ma 2016). It is noteworthy that during the occurrence of bond slip, the bond forces developed comprise of the adhesive force at the reinforcing bar-concrete interface, bearing force against the ribs of reinforcing bars, and frictional force arising from the normal action due to wedging effect. These forces would possibly induce shear failure of concrete along the reinforcing bar, formation of splitting cracks in the concrete of conical shape initiated at the edge of ribs, and splitting failure of concrete surrounding the reinforcing bar (ACI Committee 408 2003). The structural effects of such cracks are duly considered by the degradation of bond stiffness and bond stress in the constitutive model of reinforcing bar-concrete bond. This is in contrast to the concrete tensile and flexural cracks whose cracking sequence and patterns need to be determined through the crack queuing algorithm.

2.2 Crack queuing algorithm

Theoretically, the crack queuing algorithm can be applied to discrete or smeared representation of cracks with rotating or non-rotating crack model. To circumvent the need of adaptive remeshing, and to render a more realistic simulation of the non-rotating nature of cracks, the smeared approach and non-rotating crack model are adopted. Details of the crack queuing algorithm have been explicated in an earlier paper with applications to unreinforced concrete (Kwan *et al*. 1999) while this paper applies the crack queuing algorithm to capture the cracking behaviour in reinforced concrete members. Basically, it is a process whereby only one concrete element, the one most likely to crack first, is permitted to crack in each iteration step. Since a fine mesh is used for obtaining numerical results with desirable accuracy, the computed tensile stresses near the crack tips would be very high compared to the tensile strength of concrete. To avoid unstable crack propagation, the fracture toughness of concrete is introduced in formulating the cracking criterion of concrete.

An integrated concrete cracking criterion combining tensile strength and fracture toughness is defined. Consider the stress field in the neighbourhood of a crack tip, the crack propagation would follow the radial direction with maximum tangential stress σ_θ, under the condition where $\sigma_\theta(2\pi r)^{0.5}$ attains the fracture toughness of the material (Anderson 2017). In the above, r is the distance from the point being considered to the nearest crack tip. Therefore, the integrated cracking criterion is given by Eq. (1), of which the full derivation can be found from the literature (Kwan *et al*. 1999, Ma and Kwan 2015)

$$f'_{te} = \max\left(f_{te}, \frac{K_{IC}}{\sqrt{2\pi r}} \right) \tag{1}$$

where f_{te} is the tensile strength, K_{IC} is the fracture toughness, and f'_{te} is the modified tensile strength. The

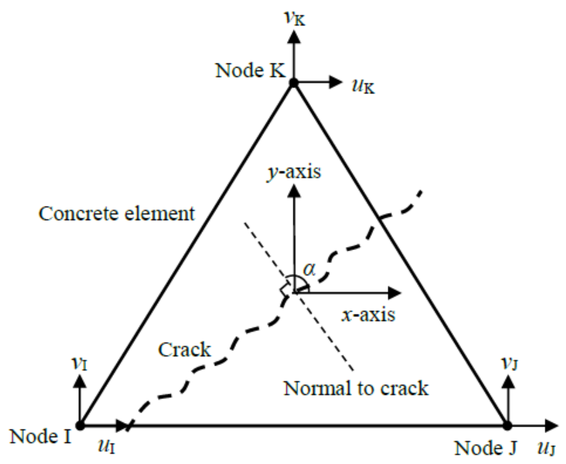

Fig. 2 Determination of crack width

introduction of fracture toughness into the cracking criterion is to allow for the singularity of stress fields at the crack tips, which often leads to very high tensile stresses in the proximity of a crack tip and uncontrollable crack propagation.

Fig. 1 depicts the flowchart of the crack queuing algorithm. In each iteration, if there is no concrete element satisfying the cracking criterion, no new crack is formed and the analysis proceeds to the next load increment. Otherwise, only the concrete element of which the maximum tensile stress exceeds the integrated cracking criterion by the greatest amount proportionately is allowed to crack. The entire structure is then re-analysed at the same loading level so as to allow the stress re-distribution to take place until convergence is achieved. This procedure is repeated until no more concrete element satisfies the integrated cracking criterion, and the analysis proceeds to the next load increment. Thus, algorithmically, the elements are queued up for cracking with respect to the integrated cracking criterion. After an element is cracked, the structure is re-analysed and the stress re-distribution may change the queue because some elements may drop out from the queue due to stress relief while some other elements may jump into the queue due to the propagation of crack tips towards them. This crack queuing process closely mimics the physical cracking behaviour of concrete.

2.3 Crack width calculation

With the adoption of the crack queuing algorithm, the computed crack pattern would much more closely resemble the actuality, and hence the crack widths could be evaluated in a more realistic manner. Due to stress re-distributions upon cracking, immediately adjacent to the crack, the tensile stresses of concrete normal to the crack plane would be negligibly small. Therefore, the crack width is determined directly from the nodal displacements of the cracked concrete element. Fig. 2 depicts a triangular concrete element whose three nodes are labelled I, J and K. The crack inside the concrete element is assumed to pass through the centroid (the assumption is reasonably accurate as far as the mesh size is not overly coarse) and the crack

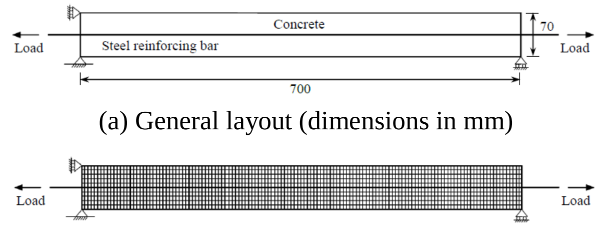

(a) General layout (dimensions in mm)

(b) Finite element mesh

Fig. 3 General layout and finite element mesh of D12-RA

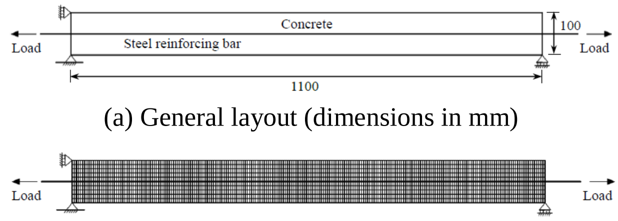

(a) General layout (dimensions in mm)

(b) Finite element mesh

Fig. 4 General layout and finite element mesh of STN-12 and STN-16

angle (angle between normal to the crack and the x-axis) is assumed to be α. Suppose there is one node (denoted by node J) on one side of the crack and the remaining two nodes (denoted by node I and node K) are on the other side of the crack. The crack width can be calculated from the relative displacements of the two nodes which are further away from the crack on opposite sides. Therefore, the crack width can be calculated from the displacement of node J from the crack d_J and the displacement of node K from the crack d_K

$$d_J = -u_J \cos\alpha - v_J \sin\alpha \tag{2a}$$

$$d_K = u_K \cos\alpha + v_K \sin\alpha \tag{2b}$$

in which u_J and v_J are the nodal displacements of node J in x- and y-directions, u_K and v_K are the nodal displacements of node K in x- and y-directions. Summing up the two displacements in Eqs. (2a) and (2b), the crack width w can be evaluated as

$$w = d_J + d_K \tag{3}$$

If the crack width so calculated is negative, the crack is regarded as closed under compression and the axial stiffness in the direction perpendicular to the crack is restored to that of uncracked concrete. The assumption that when the crack is closed, the stiffness of cracked concrete under axial compression orthogonal to the crack planes is restored to that of uncracked concrete is in line with the research findings by Vecchio and Collins (1993).

3. Concrete members analysed

Three axial tension members and one flexural member tested in the literature are analysed. The axial tension members are specimen D12-RA tested by Radnić and

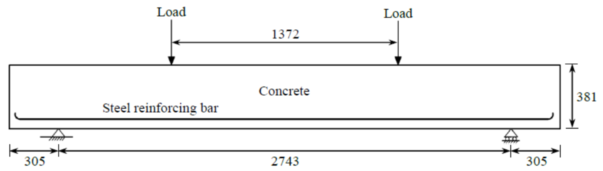

(a) General layout (dimensions in mm

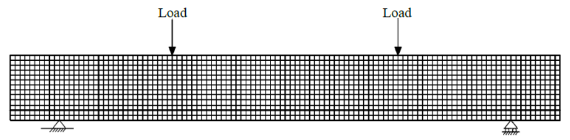

(b) Finite element mesh

Fig. 5 General layout and finite element mesh of 15-6-8-2

Table 1 Details and dimensions of specimens

Specimen number	Reference	Loading	Cross-section (mm×mm)	No of steel bars	Steel bar diameter (mm)	Steel ratio (%)
D12-RA	Radnić and Markota (2003)	Axial tension	70×70	1	12.0	2.31
STN-12	Wu and Gilbert (2009)	Axial tension	100×100	1	12.0	1.14
STN-16	Wu and Gilbert (2009)	Axial tension	100×100	1	16.0	2.05
15-6-8-2	Clark (1956)	Bending	152×381	1	25.4	1.01

Table 2 Concrete and steel properties of specimens

Specimen number	Concrete compressive strength (MPa)	Concrete tensile strength (MPa)	Concrete elastic modulus (GPa)	Steel yield strength (MPa)	Steel ultimate strength (MPa)
D12-RA	24.1	1.8	23.24	400	500
STN-12	21.6	2.0	22.40	540	600
STN-16	21.6	2.0	22.40	540	600
15-6-8-2	25.9	2.8	24.09	276	483

Notes: (1) For concrete, the Poisson's ratio is taken as 0.20.
(2) For steel, the initial elastic modulus, tensile strain at start of strain hardening and ultimate tensile strain are taken as 200 GPa, 1.0% and 10.0%, respectively.

Markota (2003) and specimens STN-12 and STN-16 tested by Wu and Gilbert (2009), whereas the flexural member is specimen 15-6-8-2 tested by Clark (1956). Each specimen is analysed by the finite element method with the crack queuing incorporated using load increments of 500 N, as well as without the crack queuing incorporated using load increments of 500 N, 50 N, 5 N and 0.5 N.

The dimensions and steel ratios of the specimens are summarized in Table 1. Specimen D12-RA has a length of 700 mm and a cross-section of 70 mm width by 70 mm depth. Only one steel bar of 12 mm diameter is embedded at the centre of specimen and the corresponding steel ratio is 2.31%. The general layout of D12-RA and the finite element mesh used in the analysis are shown in Fig. 3(a) and 3(b), respectively. Specimen STN-12 has a length of 1100 mm and a cross-section of 100 mm width by 100 mm depth. Only one steel bar of 12 mm diameter is embedded at the centre of specimen and the corresponding steel ratio is 1.14%. Specimen STN-16 has the same dimensions as STN-12, except that the embedded steel bar has a diameter of 16 mm and the corresponding steel ratio is 2.05%. The general layout of STN-12 and STN-16 and the finite element mesh are shown in Fig. 4(a) and 4(b), respectively.

Table 3 Bond properties of specimens

Specimen number	Initial bond stiffness (N/mm^3)	Peak bond stress (MPa)	Residual bond stress (MPa)	s_1 (mm)	s_2 (mm)	s_3 (mm)
D12-RA	183	9.8	1.5	0.6	0.6	1.0
STN-12	173	9.3	1.4	0.6	0.6	1.0
STN-16	173	9.3	1.4	0.6	0.6	1.0
15-6-8-2	193	10.2	1.4	0.6	0.6	1.0

Note: s_1, s_2 and s_3 are the slip at start of peak bond stress, slip at end of peak bond stress and slip at start of residual bond stress, respectively.

For specimen 15-6-8-2, the total length and span are respectively 3353 mm and 2743 mm. It has a cross-section of 152 mm width by 381 mm depth. One steel bar of 25.4 mm diameter is embedded at the position giving an effective depth of 330 mm, and the corresponding steel ratio is 1.01%. It is subjected to four-point bending and the loads are applied symmetrically at 1372 mm apart. The general layout of 15-6-8-2 and the finite element mesh are shown in Fig. 5(a) and 5(b), respectively.

The material properties of the specimens are presented in Tables 2 and 3. For the concrete properties, the compressive strength for all the specimens and the tensile strength for D12-RA, STN-12 and STN-16 are the same as those reported in the respective literature (Radnić and Markota 2003, Wu and Gilbert 2009, Clark 1956). As the tensile strength for 15-6-8-2 was not reported, it is calculated according to the formula in ACI 318 (ACI Committee 318 2014). In addition, the elastic moduli of concrete for all the three specimens are determined in accordance with ACI Committee 318 (2014), the Poisson's ratio is assumed to be 0.20, and the fracture toughness is taken as 1.3 MNm$^{-1.5}$ according to previous research (Chen *et al*. 2011). For the steel properties, the same properties as reported in the respective literature (Radnić and Markota 2003, Wu and Gilbert 2009, Clark 1956) are used. For the bond properties, the initial bond stiffness of the four specimens is evaluated according to the provisions in fib Model Code 2010 as 183, 173, 173 and 193 N/mm^3, respectively.

4. Crack pattern and crack spacing results

The four specimens are analysed by the finite element method first with crack queuing applied and then without crack queuing applied. With crack queuing applied, the load increment is fixed at 500 N, while without crack queuing applied, the load increment is successively refined in the sequence of 500 N, 50 N, 5 N and 0.5 N to study the effect of refining the load increment step size. The crack patterns for each specimen as obtained by experiment and by the finite element analyses are presented in Figs. 6 to 13, and the experimental and analytical results of crack number, crack spacing and crack widths are summarized in Tables 4 to 7.

The experimentally obtained crack patterns of D12-RA at different load levels and the corresponding analytical crack patterns with crack queuing applied are displayed in


Experimental crack pattern at load = 10 kN

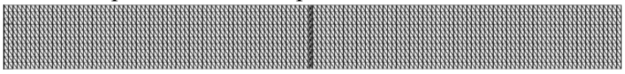
Analytical crack pattern with crack queuing at load = 11 kN


Experimental crack pattern at load = 20 kN

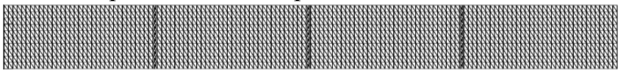
Analytical crack pattern with crack queuing at load = 20 kN


Experimental crack pattern at load = 30 kN

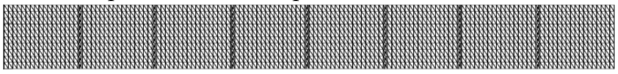
Analytical crack pattern with crack queuing at load = 30 kN

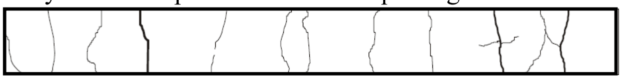
Experimental crack pattern at load = 40 kN

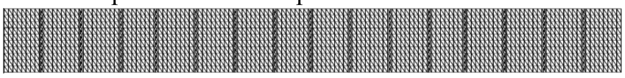
Analytical crack pattern with crack queuing at load = 40 kN

Fig. 6 Crack patterns of D12-RA at different load levels: experimental and analytical with crack queuing


Experimental crack pattern

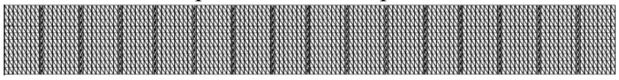
Analytical crack pattern with crack queuing (500 N load steps)

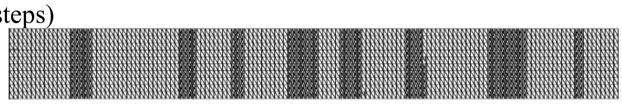
Analytical crack pattern without crack queuing (500 N load steps)

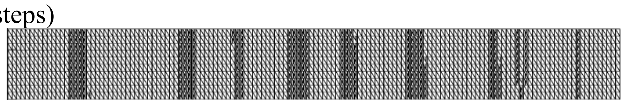
Analytical crack pattern without crack queuing (50 N load steps)

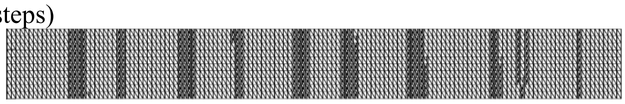
Analytical crack pattern without crack queuing (5 N load steps)

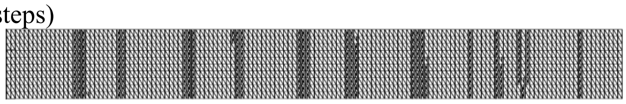
Analytical crack pattern without crack queuing (0.5 N load steps)

Fig. 7 Crack pattern of D12-RA at load = 40 kN: experimental and analytical with and without crack queuing

Fig. 6. Four cracks were observed at a load level of 10 kN during testing, while the first crack initiates at 11 kN in the finite element analysis. At a load level of 20 kN, the experimental and analytical crack numbers are 5 and 3, respectively. As the crack queuing algorithm can simulate the tension relief adjacent to a newly formed crack, the analytically obtained cracks are at finite distances away from each other, matching quite well with the real situation of having discrete cracks formed. At a higher load level of 30 kN, the experimental and analytical crack numbers are 8 and 7, respectively. At an even higher load level of 40 kN, the experimental and analytical crack numbers become 12 and 15, respectively. Overall, at low load level, the analytical crack number is less than the experimental crack number but at high load level, the analytical crack number is larger than experimental crack number.

To reveal the effects of crack queuing on D12-RA, the experimental crack pattern as well as the analytical crack patterns with and without crack queuing applied at a load level of 40 kN are compared in Fig. 7. It is seen that without crack queuing, many closely spaced cracks inside fairly wide crack bands are formed. As the load step size is refined from 500 N to 0.5 N, the number of closely spaced cracks is reduced and the crack bands become narrower. Hence, the refinement of load step size, which would lead to a smaller number of concrete elements reaching the crack criterion at one load step, could reduce the number of closely spaced cracks formed and reduce the width of crack bands. If two neighbouring cracks are counted as two cracks, the crack numbers without crack queuing using load steps of 500 N, 50 N, 5 N and 0.5 N are 38, 31, 29 and 22, respectively. These crack numbers are very different from the analytical crack number of 15 obtained with crack queuing and the experimental crack number of 12. Hence, without crack queuing, even with the load steps refined to 1/1000 times, superfluous cracks are still formed causing inaccurate predictions of crack number and spacing. Relatively, the crack queuing can produce more accurate predictions.

The crack patterns of STN-12 at a load level of 50 kN, as obtained experimentally by testing or analytically by finite element analysis with and without crack queuing applied are depicted in Fig. 8. From the figure, it can be seen that the experimental crack number and analytical crack number with crack queuing are 5 and 7, respectively. However, the analytical crack numbers without crack queuing using load steps of 500 N, 50 N, 5 N and 0.5 N are 24, 21, 18 and 14, respectively. It is evident that without crack queuing, very closely spaced cracks can be formed. Nevertheless, as the load step size is refined from 500 N to 0.5 N, the number of closely spaced cracks is reduced and the crack bands become narrower. It is only that even with the load step size refined to 1/1000 times, quite a number of superfluous cracks are still formed causing inaccurate predictions of crack number and spacing. Again, it is demonstrated that the crack queuing can produce more accurate predictions.

The experimental and analytical crack patterns of STN-16 at a load level of 105 kN are depicted in Fig. 9. From the figure, it can be seen that the experimental crack number

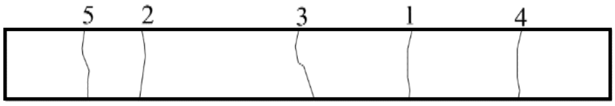

Experimental crack pattern of STN-12

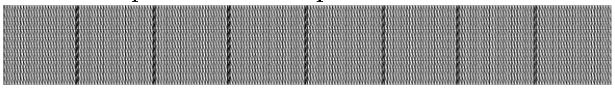

Analytical crack pattern with crack queuing (500 N load steps)

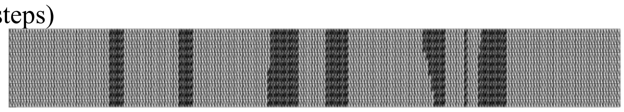

Analytical crack pattern without crack queuing (500 N load steps)

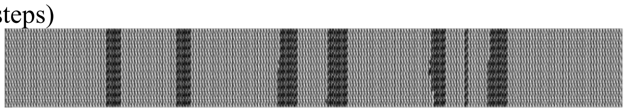

Analytical crack pattern without crack queuing (50 N load steps)

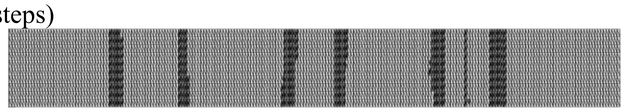

Analytical crack pattern without crack queuing (5 N load steps)

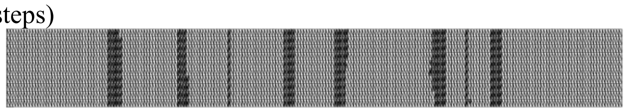

Analytical crack pattern without crack queuing (0.5 N load steps)

Fig. 8 Crack patterns of STN-12 at load = 50 kN: experimental and analytical with and without crack queuing

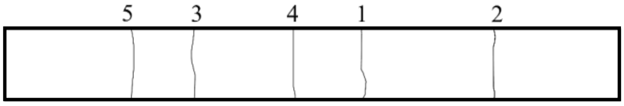

Experimental crack pattern of STN-16

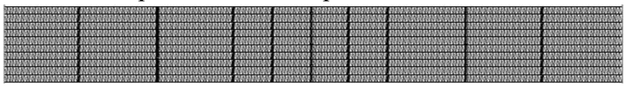

Analytical crack pattern with crack queuing (500 N load steps)

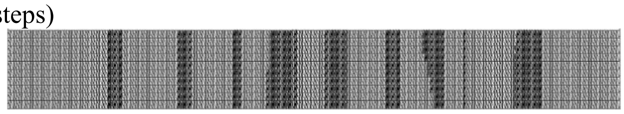

Analytical crack pattern without crack queuing (500 N load steps)

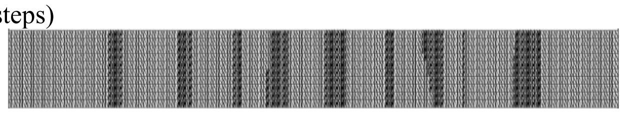

Analytical crack pattern without crack queuing (50 N load steps)

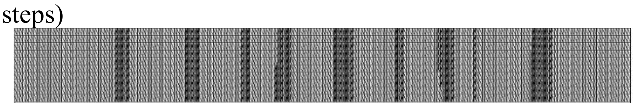

Analytical crack pattern without crack queuing (5 N load steps)

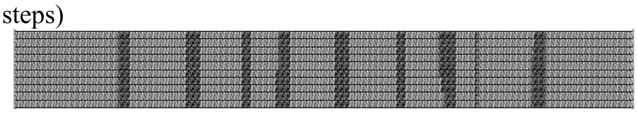

Analytical crack pattern without crack queuing (0.5 N load steps)

Fig. 9 Crack patterns of STN-16 at load = 105 kN: experimental and analytical with and without crack queuing

and analytical crack number with crack queuing are 5 and 9, respectively. In contrast, the analytical crack numbers without crack queuing using load steps of 500 N, 50 N, 5 N and 0.5 N are 30, 26, 23 and 19, respectively. Therefore, without crack queuing, the crack numbers are seriously over-estimated. As the load step size is refined from 500 N to 0.5 N, the number of closely spaced cracks is reduced and the crack bands become narrower, but not to a satisfactory extent albeit refinement of load step size to 1/1000 times.

The analytical crack patterns of 15-6-8-2 are displayed in Figs. 10 to 13. Fig. 10 shows the analytical crack patterns with crack queuing. From this figure, it can be seen that with crack queuing, the crack patterns obtained generally comprise of clearly defined discrete cracks at finite distances apart. On the other hand, Figs. 11, 12 and 13 show the analytical crack patterns without crack queuing using load steps of 500 N, 50 N and 5 N, respectively. From these figures, it is evident that with a load step size of 500 N, many closely spaced cracks inside crack bands are formed. With the load step size refined to 50 N, the number of closely spaced cracks is reduced and the crack bands become narrower. With the load step size further refined to 5 N, there are only a few superfluous cracks and each crack band becomes more like a discrete crack. Finally, with the load step size refined to 0.5 N, the crack patterns become quite similar to those obtained with crack queuing and are

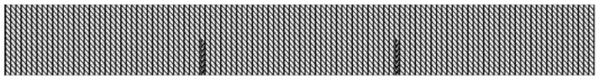

(a) Steel stress = 63 MPa

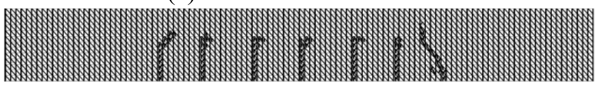

(b) Steel stress = 138 MPa

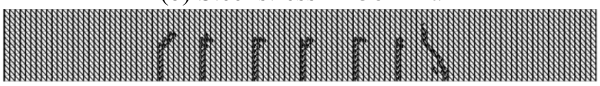

(c) Steel stress = 172 MPa

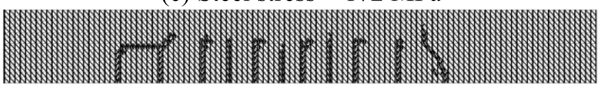

(d) Steel stress = 246 MPa

Fig. 10 Crack patterns of 15-6-8-2: analytical with crack queuing (500 N load steps)

therefore not separately presented. Overall, it appears that in the case of a concrete member subjected to bending, the number of superfluous cracks reduces more quickly as the load step size is refined than in the case of a concrete member subjected to axial tension. Nevertheless, unless the load step size is refined to 1/1000 times, finite element analysis without crack queuing is still afflicted by the formation of superfluous cracks.

From the above, it is evident that without crack queuing, a very small load step size, depending on the number of

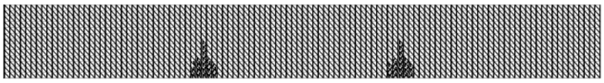

(a) Steel stress= 63 MPa

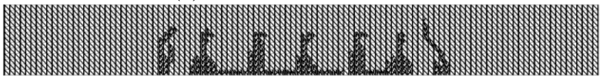

(b) Steel stress = 138 MPa

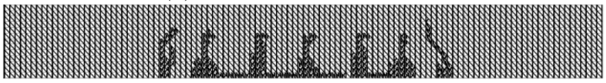

(c) Steel stress = 172 MPa

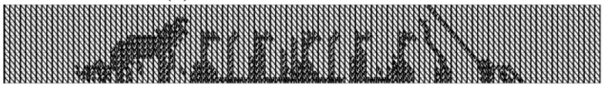

(d) Steel stress = 246 MPa

Fig. 11 Crack patterns of 15-6-8-2: analytical without crack queuing (500 N load steps)

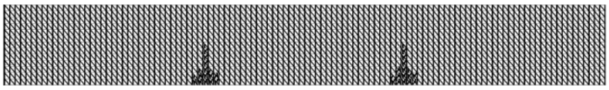

(a) Steel stress = 63 MPa

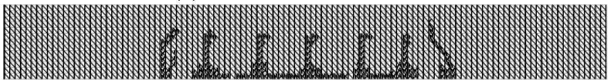

(b) Steel stress = 138 MPa

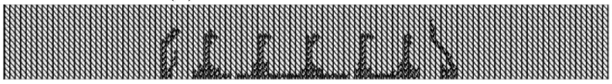

(c) Steel stress = 172 MPa

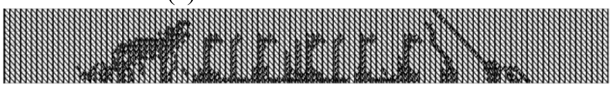

(d) Steel stress = 246 MPa

Fig. 12 Crack patterns of 15-6-8-2: analytical without crack queuing (50 N load steps)

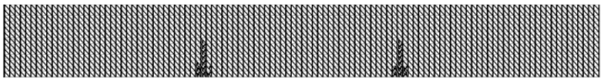

(a) Steel stress = 63 MPa

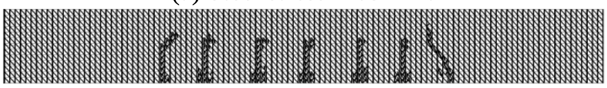

(b) Steel stress = 138 MPa

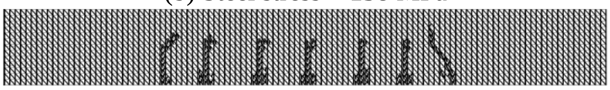

(c) Steel stress = 172 MPa

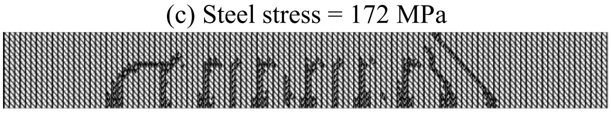

(d) Steel stress = 246 MPa

Fig. 13 Crack patterns of 15-6-8-2: analytical without crack queuing (5 N load steps)

concrete elements reaching the crack criterion at one load step, is needed for accurate analysis. Such very small load step size would however invoke enormous computational resources, as will be seen later.

Table 4 Crack number, crack spacing and crack width of D12-RA

Method of determination	Crack number	Average crack spacing (mm)	Average crack width (mm)	Maximum crack width (mm)	Computing time (hour)
Experimental	12	63	-	0.249	-
Analytical with crack queuing (500 N load steps)	15	44	0.185	0.188	5.8
Analytical without crack queuing (500 N load steps)	38	undefined	0.084	0.085	5.2
Analytical without crack queuing (50 N load steps)	31	undefined	0.091	0.092	19.5
Analytical without crack queuing (5 N load steps)	29	undefined	0.097	0.098	68.3
Analytical without crack queuing (0.5 N load steps)	22	undefined	0.128	0.129	156.3

Note: The undefined crack spacings are caused by the presence of zero spacing cracks.

Table 5 Crack number, crack spacing and crack width of STN-12

Method of determination	Crack number	Average crack spacing (mm)	Average crack width (mm)	Maximum crack width (mm)	Computing time (hour)
Experimental	5	195	0.200	0.375	-
Analytical with crack queuing (500 N load steps)	7	138	0.278	0.280	6.8
Analytical without crack queuing (500 N load steps)	24	undefined	0.084	0.086	5.7
Analytical without crack queuing (50 N load steps)	21	undefined	0.098	0.099	29.2
Analytical without crack queuing (5 N load steps)	18	undefined	0.110	0.112	71.2
Analytical without crack queuing (0.5 N load steps)	14	undefined	0.145	0.146	165.8

Note: The undefined crack spacings are caused by the presence of zero spacing cracks.

Table 6 Crack number, crack spacing and crack width of STN-16

Method of determination	Crack number	Average crack spacing (mm)	Average crack width (mm)	Maximum crack width (mm)	Computing time (hour)
Experimental	5	165	0.300	0.500	-
Analytical with crack queuing (500 N load steps)	9	104	0.270	0.275	8.4
Analytical without crack queuing (500 N load steps)	30	undefined	0.089	0.090	7.5
Analytical without crack queuing (50 N load steps)	26	undefined	0.099	0.101	36.9
Analytical without crack queuing (5 N load steps)	23	undefined	0.108	0.109	84.5
Analytical without crack queuing (0.5 N load steps)	19	undefined	0.139	0.140	189.5

Note: The undefined crack spacings are caused by the presence of zero spacing cracks.

5. Crack width results

The experimental and analytical maximum crack widths of D12-RA are plotted in Fig. 14, where the calculated crack widths per ACI 224R (ACI Committee 224 2001) and Eurocode 2 (Comité Européen de Normalisation 2004) are also plotted for comparison. It is seen that the experimental maximum crack width increases from 0.06 mm at a steel

Table 7 Crack number, crack spacing and crack width of 15-6-8-2

Method of determination	Crack number	Average crack spacing (mm)	Average crack width (mm)	Maximum crack width (mm)	Computing time (hour)
Experimental	9	157	-	0.353	-
Analytical with crack queuing (500 N load steps)	11	182	0.340	0.348	4.2
Analytical without crack queuing (500 N load steps)	21	undefined	0.180	0.183	3.8
Analytical without crack queuing (50 N load steps)	19	undefined	0.197	0.201	15.7
Analytical without crack queuing (5 N load steps)	15	undefined	0.252	0.258	40.2
Analytical without crack queuing (0.5 N load steps)	13	undefined	0.273	0.277	122.2

Note: The undefined crack spacings are caused by the presence of zero spacing cracks.

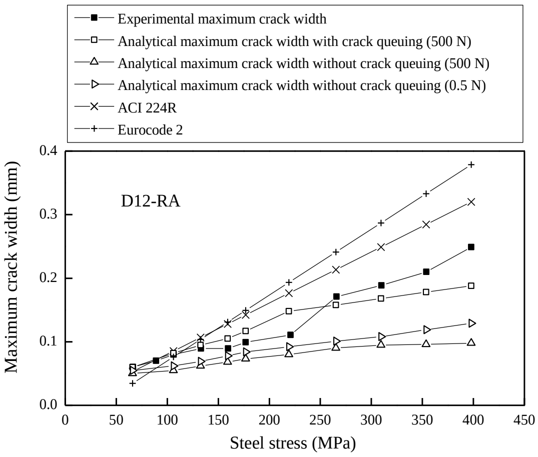

Fig. 14 Maximum crack widths of D12-RA

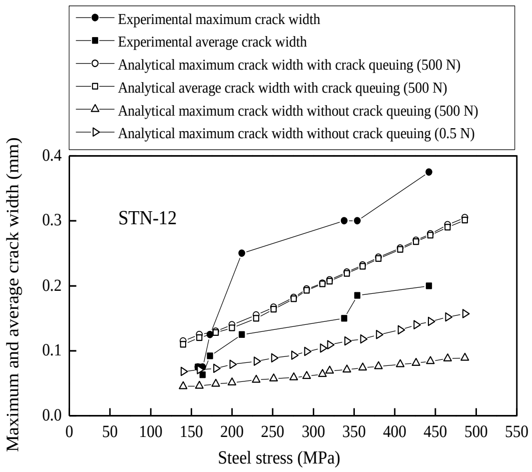

Fig. 15 Maximum and average crack widths of STN-12

stress of 66 MPa to 0.25 mm at a steel stress of 398 MPa. On the other hand, at a steel stress of 66 MPa, the analytical maximum crack widths with and without crack queuing are all about 0.05 to 0.06 mm, but at a higher steel stress of 398MPa, the analytical maximum crack widths become highly dependent on crack queuing and load step size. With

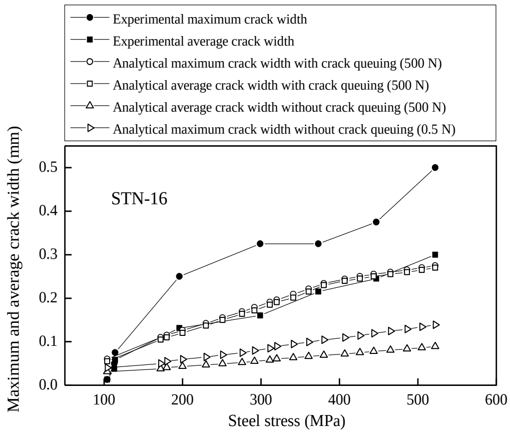

Fig. 16 Maximum and average crack widths of STN-16

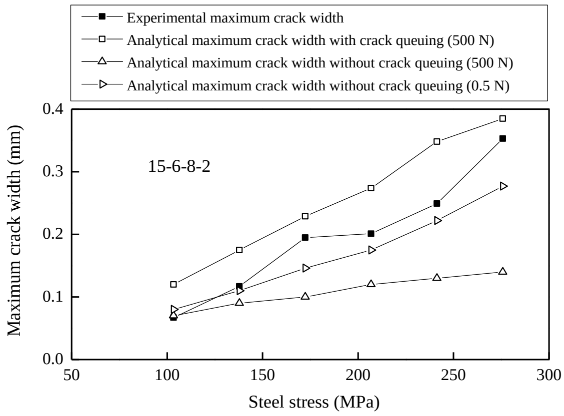

Fig. 17 Maximum crack widths of 15-6-8-2

crack queuing, the analytical maximum crack width is 0.19 mm, which is 24% smaller than the experimental maximum crack width. Without crack queuing, the analytical maximum crack widths using load steps of 500 N and 0.5 N are 0.10 mm and 0.13 mm, which are respectively 60% and 48% smaller than the experimental maximum crack width. Somehow, the calculated crack widths per ACI 224R and Eurocode 2 increase from rather small values at a relatively low steel stress to 0.32 mm and 0.38 mm respectively at a steel stress of 398 MPa. These crack widths of 0.32 mm and 0.38 mm are respectively 28% and 52% larger than the experimental maximum crack width. All in all, the maximum crack widths by finite element analysis with crack queuing are in best agreement with the experimental maximum crack width. The two design codes over-estimate the maximum crack width whereas the finite element analysis without crack queuing under-estimates the maximum crack width.

The experimental and analytical crack widths of STN-12 are presented in Fig. 15. In this figure, both the maximum and average crack widths are plotted for comparison. It is evident that the experimental maximum crack width varies from 0.08 to 0.38 mm while the experimental average crack width varies from 0.08 to 0.20 mm as the steel stress increases from 158 to 442 MPa. On the other hand, the analytical maximum crack width with crack queuing varies from 0.12 to 0.30 mm and the analytical average crack width with crack queuing varies from 0.11 to 0.29 mm as the steel stress increases from 140 to 486 MPa. These analytical maximum and average crack widths agree quite well with the respective experimental results. However, the analytical maximum crack widths without crack queuing using a load step of 500 N are only 0.05 to 0.09 mm and the analytical maximum crack widths without crack queuing using a load step of 0.5 N are only 0.07 to 0.16 mm within the same steel stress range. Hence, although the refinement of the load step size would reduce the number of superfluous cracks and thus increase the computed crack widths, even at a very small load step size of 0.5 N, the analytical maximum crack widths without crack queuing are still much too small compared to the corresponding experimental results and analytical results with crack queuing.

The experimental and analytical crack widths of STN-16 are presented in Fig. 16. Both the maximum and average crack widths are plotted for comparison. From the figure, the experimental maximum crack width varies from 0.05 to 0.50 mm while the experimental average crack width varies from 0.04 to 0.30 mm as the steel stress increases from 113 to 522 MPa. On the other hand, the analytical maximum crack width with crack queuing varies from 0.06 to 0.28 mm and the analytical average crack width with crack queuing varies from 0.06 to 0.27 mm as the steel stress increases from 104 to 522 MPa. These analytical crack widths agree reasonably well with the respective experimental results. However, the analytical maximum crack widths without crack queuing using a load step of 500 N are only 0.03 to 0.09 mm and the analytical maximum crack widths without crack queuing using a load step of 0.5 N are only 0.04 to 0.14 mm within the same steel stress range. Again, though the refinement of the load step would reduce the number of superfluous cracks and increase the computed crack widths, the resulting maximum crack widths without crack queuing are still much too small. It is therefore advocated that for crack width prediction by finite element analysis, crack queuing is a must.

The experimental and analytical maximum crack widths of 15-6-8-2 are depicted in Fig. 17. It is noted that the experimental maximum crack width varies from 0.07 to 0.35 mm as the steel stress increases from 103 to 276 MPa. In comparison, the analytical maximum crack width with crack queuing varies from 0.12 to 0.39 mm, the analytical maximum crack width without crack queuing using a load step of 500 N varies from 0.07 to 0.14 mm, and the analytical maximum crack width without crack queuing using a load step of 0.5 N varies from 0.08 to 0.28 mm, within the same steel stress range. Considering the crack widths at a steel stress of 276 MPa, the analytical maximum crack width with crack queuing is 11% larger than the experimental value, the analytical maximum crack widths without crack queuing using load steps of 500 N and 0.5 N are respectively 60% and 20% smaller than the experimental value. It is obvious that without crack queuing, the crack widths are seriously under-estimated, although refinement of the load step size would increase the computed crack widths to reduce the prediction error.

On the whole, without incorporation of the crack queuing algorithm in the finite element analysis, the crack widths would be grossly under-estimated even if the load step size is refined to 1/1000 times. Crack queuing can significantly improve the crack width predictions and is therefore highly recommended. However, it should be noted that due to spatial variation of tensile strength (in-situ concrete is never perfectly uniform), the exact crack location is dependent to some extent on the location of the weakest concrete with lowest tensile strength in the vicinity. Hence, the crack location and pattern could be quite random. In normal finite element analysis, since the exact spatial distribution of tensile strength is not known, the concrete is usually assumed to have uniform tensile strength. Nevertheless, in theory, by considering different scenarios with different spatial distributions of tensile strength in the concrete member and analysing the concrete member in the different scenarios, the ranges of crack patterns, spacings and widths can be obtained for statistical analysis. One likely outcome is that due to spatial variation of tensile strength, the crack width could fluctuate more than the case of having uniform tensile strength, thus causing the maximum crack width to be significantly larger. This explains why in all the specimens analysed, the experimental maximum crack widths are generally larger than the analytical maximum crack widths. Further research is recommended to study the possible effects of random variation in tensile strength and the statistical variations of crack pattern, spacing and width.

6. Computing time for finite element analysis

For comparing the computational efficiency of the finite element analysis with or without crack queuing applied, the computing times are summarized in the last columns of Tables 4 to 7. For the case of D12-RA, the computing time with crack queuing is 5.8 hours, and the computing times without crack queuing using load steps of 50 N, 5 N and 0.5 N are 19.5, 68.3 and 156.3 hours, respectively. As discussed previously, to obtain a satisfactory crack pattern for crack width analysis, the load step size has to be refined to 0.5 N and the corresponding computing time would be as much as 27 times that of the finite element analysis with crack queuing. For the case of STN-12, the computing time with crack queuing is 6.8 hours, and the computing times without crack queuing using load steps of 50 N, 5 N and 0.5 N are 29.2, 71.2 and 165.8 hours, respectively. To obtain a satisfactory crack pattern, the necessary refinement of the load step size to 0.5 N would increase the computing time to 24 times that of the finite element analysis with crack queuing. For the case of STN-16, the computing time with crack queuing is 8.4 hours, and the computing times without crack queuing using load steps of 50 N, 5 N and 0.5 N are 36.9, 84.5 and 189.5 hours, respectively. To obtain a satisfactory crack pattern, the necessary refinement of the load step size to 0.5 N would increase the computing time to 23 times that of the finite element analysis with crack queuing. For the case of 15-6-8-2, the computing time with crack queuing is 4.2 hours, and the computing times without crack queuing using load steps of 50 N, 5 N and 0.5 N are 15.7, 40.2 and 122.2 hours, respectively. Again, the necessary refinement of load step size to 0.5 N for accurate analysis would increase the computing time to 29 times that of the finite element analysis with crack queuing.

Summarizing, it is obvious from the above computing times and numerical results that incorporation of the crack queuing algorithm in the finite element analysis would improve not just the numerical accuracy but also the computational efficiency. For this reason, crack queuing is again highly recommended.

7. Conclusions

A nonlinear finite element analysis procedure incorporating a crack queuing algorithm for crack analysis of reinforced concrete structures has been devised. By virtue of the crack queuing algorithm, at the most only one concrete element, the one that would meet with the cracking criterion first, is allowed to crack at each iteration step, and the whole structure is re-analysed to cater for stress relief and stress re-distribution before allowing any other cracks to form. In so doing, the crack sequence and pattern can be realistically simulated, and the stress relief and stress re-distribution in the proximity of the newly formed crack can be accounted for. These would enable more accurate predictions of crack pattern, spacing and widths.

Reinforced concrete members tested under axial tension or four-point bending have been analysed and the analytical results are checked against the experimental results reported in the literature. To study the effectiveness of crack queuing, the analysis is first carried out with crack queuing applied and then again without crack queuing applied. It is found that with crack queuing applied, the computed crack pattern, spacing and widths all agree well with the respective experimental results. However, without crack queuing applied, due to inability to allow for stress relief and re-distribution upon cracking, many closely spaced superfluous cracks are formed, leading to generation of unrealistic crack pattern, over-estimation of crack number and under-estimation of crack widths. Although refinement of the load step size would reduce the number of superfluous cracks and increase the computed crack widths to agree better with the experimental results, this would increase the computing time by many times. Incorporation of crack queuing is a more rational approach and is computationally more efficient to avoid excessive refinement of load step size.

Acknowledgments

The support from the Marie Skłodowska-Curie Actions Fellowship of the European Commission (Project No. 751461) is gratefully acknowledged.

References

ACI Committee 224 (2001), *ACI 224R-01: Control of Cracking in Concrete Structures*, American Concrete Institute, Farmington Hills, Michigan, U.S.A.

ACI Committee 318 (2014), *ACI 318R-14: Building Code Requirements for Structural Concrete*, American Concrete Institute, Farmington Hills, Michigan, U.S.A.

ACI Committee 408 (2003), *ACI 408R-03: Bond and Development of Straight Reinforcing Bars in Tension*, American Concrete Institute, Farmington Hills, Michigan, U.S.A.

Anderson, T.L. (2017), *Fracture Mechanics: Fundamentals and Applications*, 4th Edition, CRC Press, Boca Raton, Florida, U.S.A.

Azevedo, N.M., Lemos, J.V. and Almeida, J.R. (2010), "A discrete particle model for reinforced concrete fracture analysis", *Struct. Eng. Mech.*, **36**(3), 343-361.

Bažant, Z.P. and Oh, B.H. (1983), "Crack band theory for fracture of concrete", *Mater. Struct.*, **16**(3), 155-177.

Bittencourt, T.N., Wawrzynek, P.A., Ingraffea, A.R. and Sousa, J.L. (1996), "Quasi-automatic simulation of crack propagation for 2D LEFM problems", *Eng. Fract. Mech.*, **55**(2), 321-334.

Bobiński, J. and Tejchman, J. (2012), "Application of extended finite element method to cracked concrete elements-numerical aspects", *Arch. Civil Eng.*, **58**(4), 409-431.

Červenka, V. (1985), "Constitutive model for cracked reinforced concrete", *ACI J. Proc.*, **82**(6), 877-882.

Chen, G. and Baker, G. (2004), "Analysis of crack spacing in reinforced concrete by a lattice model", *Adv. Struct. Eng.*, **7**(2), 179-187.

Chen, H.H., Su, R.K.L. and Kwan, A.K.H. (2011), "Fracture toughness of plain concrete made of crushed granite aggregate", *Trans. Hong Kong Inst. Eng.*, **18**(2), 6-12.

Chen, S., Yue, Z.Q. and Kwan, A.K.H. (2013), "Actual microstructure-based numerical method for mesomechanics of concrete", *Comput. Concrete*, **12**(1), 1-18.

Clark, A.P. (1956), "Cracking in reinforced concrete flexural members", *ACI J. Proc.*, **52**(4), 851-862.

Comité Européen de Normalisation (2004), *Eurocode 2: Design of Concrete Structures: Part 1-1: General Rules and Rules for Buildings*, British Standards Institution, London, U.K.

Contrafatto, L., Cuomo, M. and Fazio, F. (2012), "An enriched finite element for crack opening and rebar slip in reinforced concrete members", *Int. J. Fract.*, **178**(1), 33-50.

Cusatis, G., Mencarelli, A., Pelessone, D. and Baylot, J.T. (2010), "The lattice discrete particle model (LDPM) for the simulation of uniaxial and multiaxial behavior of concrete: Recent results", *Proceedings of the 7th International Conference on Fracture Mechanics of Concrete and Concrete Structures*, Seoul, Korea.

De Borst, R. and Nauta, P. (1985), "Non-orthogonal cracks in a smeared finite element model", *Eng. Comput.*, **2**(1), 35-46.

Desayi, P. and Krishnan, S. (1964), "Equation for the stress-strain curve of concrete", *ACI J. Proc.*, **61**(3), 345-350.

Eliáš, J. and Stang, H. (2012), "Lattice modeling of aggregate interlocking in concrete", *Int. J. Fract.*, **175**(1), 1-11.

Fédération Internationale du Béton (2013), *fib Model Code for Concrete Structures*, Ernst & Sohn, Berlin, Germany.

Frantzeskakis, C. and Theillout, J.N. (1989), "Nonlinear finite element analysis of reinforced concrete structures with a particular strategy following the cracking process", *Comput. Struct.*, **31**(3), 395-412.

Goodman, R.E., Taylor, R.L. and Brekke, T.L. (1968), "A model for the mechanics of jointed rock", *J. Soil Mech. Foundat. Div.*, **94**(3), 637-659.

Gupta, A.K. and Akbar, H. (1984), "Cracking in reinforced concrete analysis", *J. Struct. Eng.*, **110**(8), 1735-1746.

Ingraffea, A.R. and Saouma, V. (1985), *Numerical Modeling of Discrete Crack Propagation in Reinforced and Plain Concrete, Fracture Mechanics of Concrete: Structural Application and Numerical Calculation*, Springer Netherlands.

Jendele, L. and Červenka, J. (2006), "Finite element modelling of reinforcement with bond", *Comput. Struct.*, **84**(28), 1780-1791.

Khodaie, S., Matta, F. and Alnaggar, M. (2016), “Lattice discrete particle modeling of shear failure in scaled GFRP reinforced concrete beams without stirrups”, *Proceedings of the 9th International Conference on Fracture Mechanics of Concrete and Concrete Structures*, Berkeley, California, U.S.A.

Kupfer, H.B. and Gerstle, K.H. (1973), “Behavior of concrete under biaxial stresses”, *J. Eng. Mech. Div.*, **99**(4), 853-866.

Kwan, A.K.H. (1999), “Finite element analysis of micro-crack propagation in concrete”, *Proceedings of the 4th Asia-Pacific Conference on Computational Mechanics*, Singapore.

Kwan, A.K.H. and He, X.G. (2001), “Finite element analysis of effect of concrete confinement on behaviour of shear walls”, *Comput. Struct.*, **79**(19), 1799-1810.

Kwan, A.K.H. and Ma, F.J. (2016), “Crack width analysis of reinforced concrete members under direct tension by finite element method and crack queuing algorithm”, *Eng. Struct.*, **126**(1), 618-627.

Kwan, A.K.H., Leung, A.Y.T. and Ng, P.L. (2010), “Adaptive constrained mesh generation: Part 2-accommodation of constraints”, *Int. J. Appl. Math. Mech.*, **6**(8), 22-45.

Kwan, A.K.H., Ng, P.L. and Wang, Z.M. (2017), “Mesoscopic analysis of crack propagation in concrete by nonlinear finite element method with crack queuing algorithm”, *Proc. Eng.*, **172**, 620-627.

Kwan, A.K.H., Wang, Z.M. and Chan, H.C. (1999), “Mesoscopic study of concrete II: Nonlinear finite element analysis”, *Comput. Struct.*, **70**(5), 545-556.

Ma, F.J. and Kwan, A.K.H. (2015), “Crack width analysis of reinforced concrete members under flexure by finite element method and crack queuing algorithm”, *Eng. Struct.*, **105**(1), 209-219.

Mander, J.B. (1983), *Seismic Design of Bridge Piers*, Ph.D. Dissertation, University of Canterbury, New Zealand.

Moës, N. and Belytschko, T. (2002), “Extended finite element method for cohesive crack growth”, *Eng. Fract. Mech.*, **69**(7), 813-833.

Ng, P.L., Kwan, A.K.H. and Leung, A.Y.T. (2010), “Adaptive constrained mesh generation: Part 1-stripwise advancing front technique”, *Int. J. Appl. Math. Mech.*, **6**(8), 1-21.

Ng, P.L., Lam, J.Y.K. and Kwan, A.K.H. (2011), “Effects of concrete-to-reinforcement bond and loading conditions on tension stiffening”, *Proc. Eng.*, **14**, 704-714.

Ng, P.L., Ma, F.J. and Kwan, A.K.H. (2015), “Crack analysis of concrete beams based on pseudo-discrete crack model”, *Proceedings of the 2nd International Conference on Performance-Based and Life-Cycle Structural Engineering*, Brisbane, Australia.

Ngo, D. and Scordelis, A.C. (1967), “Finite element analysis of reinforced concrete beams”, *ACI J. Proc.*, **64**(3), 152-163.

Nilson, A.H. (1968), “Nonlinear analysis of reinforced concrete by the finite element method”, *ACI J. Proc.*, **65**(9), 757-766.

Ohmenhäuser, F., Weihe, S. and Kröplin, B. (1998), “Classification and algorithmic implementation of smeared crack models”, *Proceedings of the Computational Modelling of Concrete Structures*, Badgastein, Austria, Balkema, Rotterdam, the Netherlands.

Radnić, J. and Markota, L. (2003), “Experimental verification of engineering procedures for calculation of crack width in concrete elements”, *Int. J. Eng. Modell.*, **16**(1), 63-69.

Rashid, Y.R. (1968), “Ultimate strength analysis of prestressed concrete pressure vessels”, *Nucl. Eng. Des.*, **7**(4), 334-344.

Roth, S.N., Léger, P. and Soulaïmani, A. (2013), “XFEM using a non linear fracture mechanics approach for concrete crack propagation in dam safety assessment”, *Proceedings of the 8th International Conference on Fracture Mechanics of Concrete and Concrete Structures*, Toledo, Spain.

Roth, S.N., Léger, P. and Soulaïmani, A. (2015), “A combined XFEM-damage mechanics approach for concrete crack propagation”, *Comput. Meth. Appl. Mech. Eng.*, **283**, 923-955.

Rots, J.G., Nauta, P., Kuster, G.M.A. and Blaauwendraad, J. (1985), “Smeared crack approach and fracture localization in concrete”, *Heron*, **30**(1), 1-48.

Schlangen, E. and Garboczi, E.J. (1997), “Fracture simulations of concrete using lattice models: Computational aspects”, *Eng. Fract. Mech.*, **57**(2-3), 319-332.

Schlangen, E. and Van Mier, J.G.M. (1992), “Simple lattice model for numerical simulation of fracture of concrete materials and structures”, *Mater. Struct.*, **25**(9), 534-542.

So, M., Harmon, T.G. and Dyke, S. (2010), “FEA implementation of smeared cyclic bond slip-based two-dimensional membrane model”, *ACI Struct. J.*, **107**(1), 92-100.

Suidan, M. and Schnobrich, W.C. (1973), “Finite element analysis of reinforced concrete”, *J. Struct. Div.*, **99**(10), 2109-2122.

Vecchio, F.J. and Collins, M.P. (1993), “Compression response of cracked reinforced concrete”, *J. Struct. Eng.*, **119**(12), 3590-3610.

Wang, Z.M., Kwan, A.K.H. and Chan, H.C. (1999), “Mesoscopic study of concrete I: generation of random aggregate structure and finite element mesh”, *Comput. Struct.*, **70**(5), 533-544.

Wells, G.N. and Sluys, L.J. (2001), “A new method for modelling cohesive cracks using finite elements”, *Int. J. Numer. Meth. Eng.*, **50**(12), 2667-2682.

Willam, K. and Pramono, E. (1987), “Fundamental issues of smeared crack models”, *Proceedings of the SEM/RILEM International Conference of Fracture of Concrete and Rock*, Houston, Texas, U.S.A.

Wu, H.Q. and Gilbert, R.I. (2009), “Modeling short-term tension stiffening in reinforced concrete prisms using a continuum-based finite element model”, *Eng. Struct.*, **31**(10), 2380-2391.

Yang, Z.J. and Chen, J.F. (2005), “Finite element modelling of multiple cohesive discrete crack propagation in reinforced concrete beams”, *Eng. Fract. Mech.*, **72**(14), 2280-2297.

CC